

NUMERICAL STUDY OF VORTEX-INDUCED MOTIONS OF A BUOYANCY CAN IN CURRENTS

XIE KANGDI ¹, ZHAO WEIWEN ², WAN DECHENG ³

^{1,2,3}*Collaborative Innovation Center for Advanced Ship and Deep-Sea Exploration, State Key Laboratory of Ocean Engineering, School of Naval Architecture, Ocean and Civil Engineering, Shanghai Jiao Tong University, Shanghai 201306, China* ³*Corresponding Author: dcwan@sjtu.edu.cn*

Keywords: Buoyancy can, DDES, overset grid, vortex-induced motions.

Buoyancy cans in typical cylindrical shape are widely applied in deep-water fields to tension a riser and keep it vertical^[1]. Flow over a buoyancy can induces an alternating vortex shedding, which leads to the surge, sway and yaw motions. Recent studies concentrate on the motion characteristics of Spar platforms and semi-submersible platforms, while few researchers push forward the investigation into the VIM (vortex-induced motion) phenomenon especially the yaw motion of the typical cylindrical object. Therefore, the buoyancy can in typical cylindrical shape is a suitable object to reveal the mechanism of VIM phenomenon.

Numerical simulation is an effective method to investigate the VIM issues, and numerical tests have fit well with the experimental results in vortex-induced motion of the platform. Etienne and Fontaine ^[2] conducted a 2D (two-dimensional) numerical simulation to study the motion trajectory of the cylinder after releasing the rotational degree of freedom. Minguez et al. ^[3, 4] presented a slender buoyancy can flow-induced response at high Reynolds number and 2D CFD (computational fluid dynamic) model is built to investigate the yaw responses of the buoyancy can.

The aim of this paper is to present 3D CFD model to analyse the FIR (flow-induced response) especially the yaw motion of a buoyancy can and illustrate the relationship between the yaw motion and the motion in the inline and cross flow directions. Furthermore, the influence level of release in the degree of rotation is also illustrated in this paper.

In this paper, a DDES (delayed detached-eddy simulation) method based on the SST (shear-stress transport) model is used to simulate the turbulence detached flow during a large range of high Reynolds numbers ^[5]. SST-DDES is a hybrid RANS (Reynolds-Averaged Navier-Stokes)-LES (large eddy simulation) method. It utilizes sub-grid scale model to handle the flow in the free shear flow area far away from wall, and employs RANS's SST model to solve the flow in the boundary layer near wall and other areas. This can guarantee the accuracy of LES solution, and reduce the amount of calculation in the near-wall region of the boundary layer. For incompressible viscous fluids, the continuity equation and momentum equation can be expressed as:

$$\frac{\partial \bar{u}_i}{\partial x_i} = 0 \quad (1)$$

$$\frac{\partial \bar{u}_i}{\partial t} + \frac{\partial \bar{u}_j \bar{u}_i}{\partial x_j} = \frac{\partial \bar{P}}{\partial x_i} + \frac{\partial}{\partial x_j} \left[v \left(\frac{\partial \bar{u}_i}{\partial x_j} + \frac{\partial \bar{u}_j}{\partial x_i} \right) \right] - \frac{\partial \tau_{ij}}{\partial x_j} \quad (2)$$

where, v is the molecular viscosity, τ_{ij} is the Reynolds stress or sub-grid stress tensor. According to the Boussinesq hypothesis, τ_{ij} can be expressed as:

$$\tau_{ij} = \frac{2}{3} \delta_{ij} k - v_t \left(\frac{\partial \bar{u}_i}{\partial x_j} + \frac{\partial \bar{u}_j}{\partial x_i} \right) \quad (3)$$

SST-DDES turbulence model assumes that the turbulent viscosity v_t can be expressed as a function of turbulent kinetic energy k , turbulence dissipation rate ω and velocity strain S ^[6]:

$$v_t = \frac{a_1 k}{\max(a_1 \omega, SF_2)} \quad (4)$$

where, k and ω can be obtained by solving the corresponding transport equation:

$$\frac{\partial k}{\partial t} + \frac{\partial (u_j k)}{\partial x_j} = \tilde{G} - \frac{k^{\frac{3}{2}}}{l_{DDES}} + \frac{\partial}{\partial x_j} \left[(v + \alpha_k v_t) \frac{\partial k}{\partial x_j} \right] \quad (5)$$

$$\frac{\partial \omega}{\partial t} + \frac{\partial (u_j \omega)}{\partial x_j} = \gamma S^2 - \beta \omega^2 + \frac{\partial}{\partial x_j} \left[(v + \alpha_\omega v_t) \frac{\partial \omega}{\partial x_j} \right] - (1 - F_1) CD_{k\omega} \quad (6)$$

The l_{DDES} in Eq. (5) is the mixed length, which is the switch that controls the transformation between LES and RANS model^[5].

The computational model in this paper is the model in the towing experiment delivered by KANG et al.^[7] The model of the buoyancy can is in typical cylindrical shape and detail parameters of the buoyancy can are shown in Table 1.

As shown in Fig. 1, the overall buoyancy can is underwater regardless of the free surface issue. The buoyancy can is connected with a mooring line at the centre of the bottom of the model, fairlead point. And the anchor point is outside the computational domain.

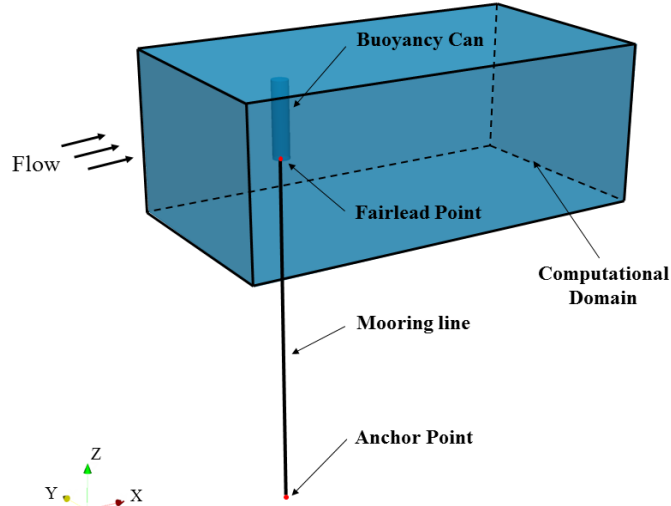


Figure 1: Schematic diagram of computational model

Table 1: Parameters of the buoyancy can

Parameter	Unit	Value
Outer diameter (D)	mm	150
Length (L)	mm	700
Displacement (Δ)	Kg	12.37
Weight (w)	Kg	4.24

Since the overset grid is applied in the cases, there are two kinds of mesh, one is cylinder grid, the other is background grid. Both grids are structured grid and the vicinity of the cylinder is locally refined as Fig. 3a shows. In cylinder grid region, the grid size near the wall is set to be small to obtain more accurate flow separation and y^+ is about 5. And the grid number of background grid region is 0.71 million, while that of cylinder grid region is 1.62 million. Fig. 3b shows the local mesh distribution of cylinder at the $z = 0$ section. The boundary conditions of the computational domain are set as follow: free stream velocity for inlet, pressure equals zero for outlet, symmetry for top, slip for other side patches.

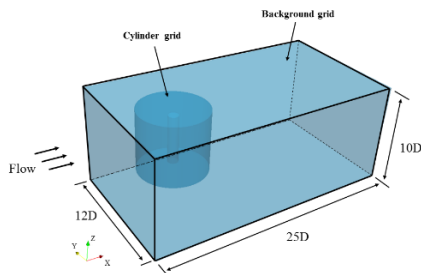


Fig. 2 Computational domain

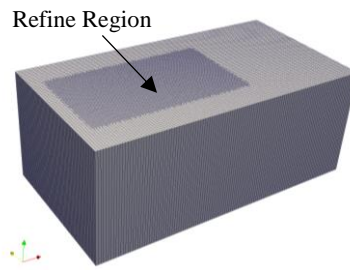


Fig.3 Overall computational mesh

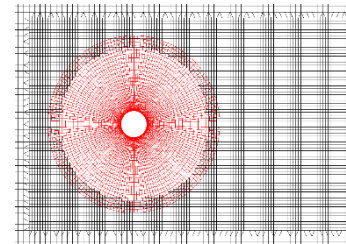


Fig.4 Local mesh

In free decay test case, the buoyancy can under no incoming flow is given an initial velocity and released to get the natural period of the mooring system. Since the consecutive VIM numerical tests are under the condition that the length of mooring line is 2.672 m, the numerical free decay test keeps the same length of the mooring line. After the Fourier transform, it shows that the CFD result fits well with the KANG et al.'s^[6] experimental result as Fig. 5 presents:

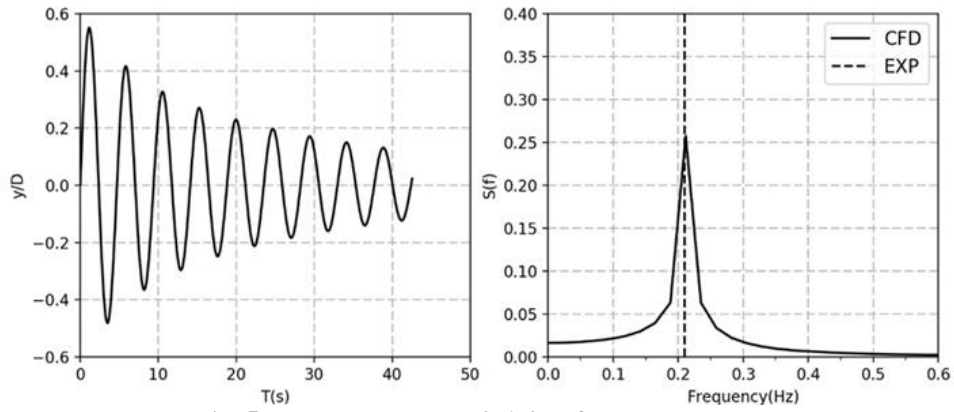


Fig. 5 Tether length $L = 2.672$ m free decay result

With the increase of reduced velocity, the average surge displacement and surge and sway frequency of the buoyancy can are increased significantly. In general, when the vortex shedding is stable, the motion trajectory becomes regular in “8” shape. The internal mechanism of the special shape is that the surge frequency is twice of the sway frequency just as Fig. 6 presents.

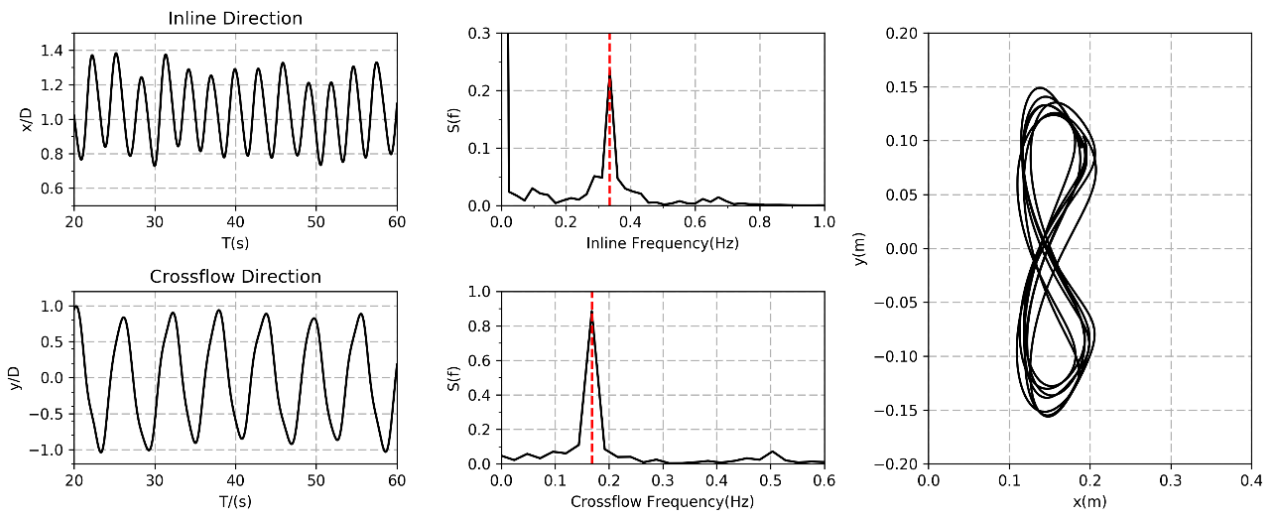


Fig. 6 Time-Displacement profile & Fourier transform profile & Motion trajectory ($U_r = 6$)

In this paper, this numerical method can obviously capture the rotation phenomenon of the buoyancy can in the uniform flow as Fig. 7 presents.

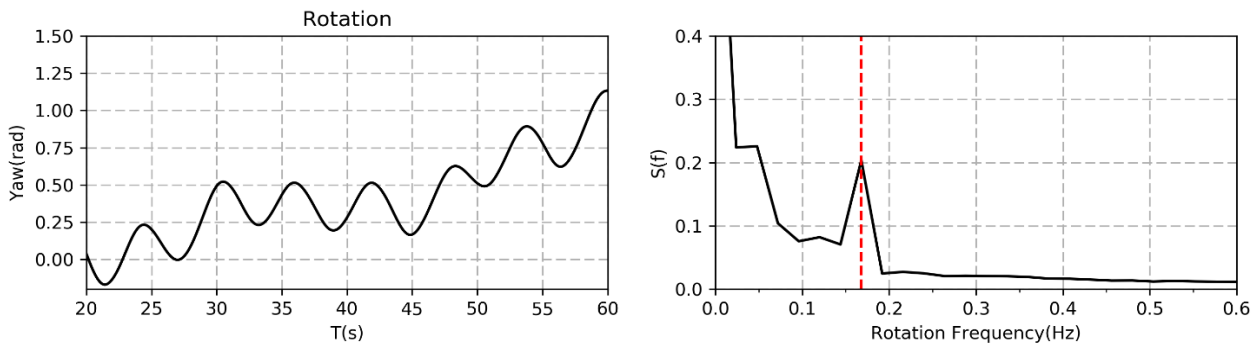


Fig. 7 Time-rotation profile & Fourier transform profile ($U_r = 6$)

According to Table 2, same as surge and sway frequency, the yaw frequency increases with the increase of reduced velocity. Secondly, yaw frequency is equal to the sway frequency, which is consistent with KANG et al.’s [6] experimental result. The reason for this circumstance is that the sway motion and yaw motion are both caused by the vortex shedding. It can infer that the sway motion and yaw motion share the same exciting force component.

Table 2: Surge frequency, sway frequency and yaw frequency

Reduced velocity (U_r)	Surge frequency/Hz	Sway frequency/Hz	Yaw frequency/Hz
4	0.303	0.151	-
6	0.336	0.168	0.168
7	0.376	0.182	0.182
8	0.428	0.214	0.214
10	0.498	0.249	0.249

Acknowledgements

The authors thank all those involved in the organisation of OFW13 and to all the contributors that will enrich this event.

References

- [1] Karunakaran, D., Lee, D., and Mair, J. 2009. Qualification of the Grouped SLOR Riser System. In Proceedings of the Offshore Technology Conference, 4-7.
- [2] Etienne, S., and Fontaine, E. 2010. Effect of Rotational Degree of Freedom on Vortex-Induced Vibrations of a Circular Cylinder in Cross-Flow. In Proceedings of the 20th International Offshore and Polar Engineering Conference, 20-5.
- [3] Minguez, M., Luppi, A., and Berger, A. 2012. Slender Buoy FSHR Vortex Induced Rotations. In Proceedings of the ASME 31st International Conference on Ocean, Offshore and Arctic Engineering, 713-22.
- [4] Minguez, M., Luppi, A., Pattedoie, S., and Maloberti, R. 2011. Slender Buoy VIM and VIR Analysis by CFD/FSI Approach. In Proceedings of the ASME 30th International Conference on Ocean, Offshore and Arctic Engineering, 1-9.
- [5] ZHAO, W. W., and WAN, D. C. 2016. Detached-Eddy Simulation of Flow past Tandem Cylinders. Applied Mathematics and Mechanics 37 (12): 1272-81.
- [6] Menter, F. R., Kuntz, M., and Langtry, R. 2003. Ten Years of Industrial Experience with the SST Turbulence Model. In Proceedings of the 4th International Symposium on Turbulence Heat and Mass Transfer, 625-32.
- [7] KANG, Z., NI, W. C., MA, G., and XU, X. 2017. A Model Test Investigation on Vortex-Induced Motions of a Buoyancy Can. Marine Structures 53: 86-104.